Oriented Crystallization in Polypropylene Fibers Induced by a Sorbitol-Based Nucleator

Jonathan Lipp,[†] Michael Shuster,[‡] Gavin Feldman,[‡] and Yachin Cohen*[,†]

Department of Chemical Engineering and the Russell Berrie Institute for Nanotechnology, Technion—Israel Institute of Technology, Technion City, Haifa 32000, Israel, and Carmel Olefins Ltd., P.O. Box 1468, Haifa 31014, Israel

Received June 21, 2007; Revised Manuscript Received October 23, 2007

ABSTRACT: The role of 1,3:2,4-di(3,4-dimethylbenzylidene)sorbital (DMDBS) in inducing oriented crystallization during the melt spinning of polypropylene (PP) fibers has been investigated, regarding the tensile properties and crystal orientation (WAXS, SAXS) of the fibers. Better orientation and higher Young's modulus were obtained at a content of 0.4% (w/w) DMDBS, under conditions in which the DMDBS nanofibrils are fully developed in the PP melt. It is suggested the nanofibrils, oriented by the shear and elongational flow prior to PP crystallization, serve as nucleation centers for its subsequent crystallization.

1. Introduction

Polymer fibers have gained, over the years, abundant usage in a variety of applications from apparel to industrial fabric. Polypropylene (PP) is among the most commonly used polymers in fiber manufacture. Enhancement of fiber properties while reducing its cost is an ongoing technological endeavor. One route in this direction is the use of additives. Much used additives in PP are clarifiers based on dibenzylidene sorbitol (DBS). These substances have been studied intensively due to their ability to self-associate in organic solvents[1] and polymer melts[2−4] to yield a fibrillar network[4−6] that gels the matrix and nucleates semicrystalline polymers.[4] The accepted mechanism for nucleation includes dissolution of DBS in the polymer melt at a high temperature followed by fibrillar structure formation upon initial cooling. These structures epitaxially nucleate polymer crystallization upon further cooling.[7] Clarification stems from significant reduction of the crystallites' size as a result of the nucleation. Investigations of DBS-based nucleators in PP indicated that at low additive content (up to about 0.5%) clarity is enhanced, an effect that is lost when the content exceeds 2%.[8] Mechanical properties, such as Young's modulus of injection-molded samples, increase with additive content up to 0.75%.[9]

The influence of DBS and its derivatives on the orientation achieved during processing of semicrystalline polymers has also been investigated. Enhancement of shear-induced orientation by the presence of DBS fibrils was indicated.[10−13] The fibrils align parallel to the applied shear while polymer crystals grow epitaxially on the fibril surface, perpendicular to the shear direction.[10] Increasing the shear rate or DBS content (measured up to 5%) enhances polymer crystal orientation.[11] While previous studies addressed the effect of sorbitol derivatives on shear-induced polymer orientation, the effect on elongational flow, such as in fiber melt spinning, has not yet been studied. The patent literature teaches extrusion of PP fibers that include nucleating agents which are able to be drawn at high ratios to achieve enhanced values of tensile modulus and strength.[14,15] It is therefore the aim of this work to investigate the influence of DBS derivatives at different concentrations on PP fiber morphology and properties. In particular, we focus on the effect of processing conditions by which the nucleator fibrils are present intact during the flow of the polymer melt, thus serving as oriented nucleation sites for subsequent polymer crystallization. The specific representative of the DBS family used in this study was 1,3:2,4-di(3,4-dimethylbenzylidene)sorbitol (DMDBS), as seen in Figure 1.

2. Experimental Section

2.1. Materials. Commercial grade PP (Capilene QT−Carmel Olefins Ltd., a random propylene copolymer with 4% ethylene, MFR 25) was used. DMDBS (Millad 3988, Milliken Inc.) was used as received. PP compounds containing 0.4 and 1 wt % DMDBS and a reference sample containing no additive were prepared. The components were melt processed using a Prism laboratory compounder at 220 °C. This processing temperature is high enough to ensure complete melting of the DMDBS. The compounds were melt-spun from a Rosand capillary rheometer with a 15 mm piston diameter and a circular die, 20 mm long and 2 mm in diameter, to produce PP monofilaments differing in DMDBS concentration and diameters. The piston speed was kept constant at 5 mm/min while two discrete take-up speeds were used; nominally at 5 and 50 m/min these correspond to spin draw ratios (SDR) of about 18 and 180 (neglecting die swell).

Preliminary experiments have shown that at concentrations 0.4−1.0 wt % melting of the fibrillar structures within PP melt takes place at ∼200 °C. In order to differentiate between the effect of preexisting and in situ formed fibrillar structures, two temperature protocols (TP) were used, differing in the temperature at which the melt was held in the piston: (a) 10 min at 220 °C (in order to dissolve DMDBS in the melt) under contact pressure and subsequently a decrease to 180 °C for the spinning process (TP1); (b) a constant temperature of 180 °C throughout, in order to keep the DMDBS fibrillar structure, formed within PP during the compounding step, intact (TP2).

2.2. Small- and Wide-Angle X-ray Scattering. Small-angle X-ray scattering (SAXS) and wide-angle X-ray scattering (WAXS) measurements were conducted to evaluate the orientation and crystallinity of the spun fibers at room temperature. Measurements were performed using a small-angle diffractometer (Bruker Nanostar, KFF CU 2 K-90) with Cu K_α radiation from a sealed tube, two Göbel mirrors and two-pinhole collimation (that result in a beam about 300 μm in diameter on the sample), and a 10 × 10 cm^2 two-dimensional position-sensitive wire detector that is positioned 65 cm behind the examined sample for SAXS evaluations and 6.7 cm for WAXS ones. The samples were mounted on an aluminum sample holder and were introduced to the vacuum chamber,

* To whom correspondence should be addressed: Fax +972 482 92 850; e-mail yachinc@tx.technion.ac.il.
[†] Technion—Israel Institute of Technology.
[‡] Carmel Olefins Ltd.

10.1021/ma071387u CCC: $40.75
Published on Web 12/11/2007

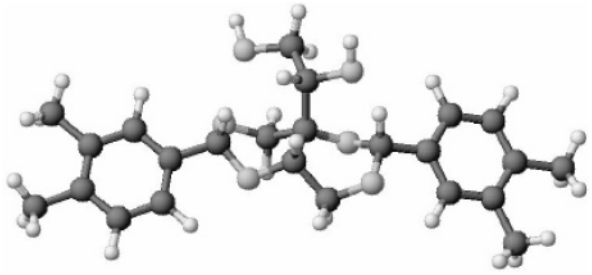

Figure 1. 3D optimization of DMDBS chemical structure (darker atoms are carbon, light gray ones are oxygen, and the white atoms are hydrogen).

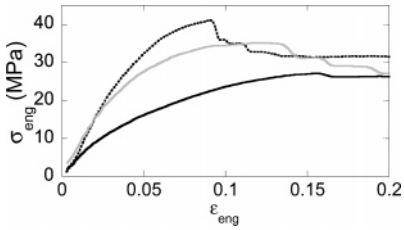

Figure 2. Stress−strain curves (average of five samples) measured for fibers fabricated using TP2 with low SDR, where the solid black, the gray, and the dashed lines were taken for 0, 1, and 0.4% DMDBS, respectively.

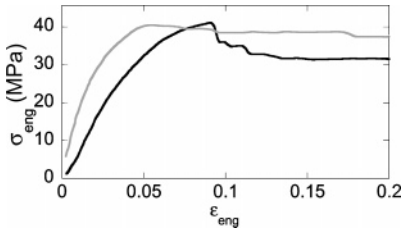

Figure 3. Stress−strain curves (average of five samples) measured for fibers, containing 0.4% DMDBS, fabricated using TP2, where the black and gray lines indicate, low and high SDR, respectively.

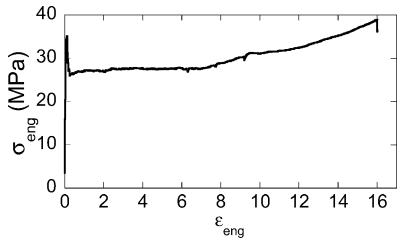

Figure 4. Stress−strain curve (average of five samples) measured for fibers, containing 1% DMDBS, fabricated using TP2 with low SDR.

perpendicular to the incident beam. In this apparatus the exposure time was 18 h for SAXS and 2 h for WAXS.

2.3. Mechanical Properties. Evaluation of the Young's moduli was carried out using a LFplus LLOYD tensile machine equipped with a 50 N load. All samples were examined at draw speed of 20 mm/min. Five or more measurements were repeated for each sample, and then linear regressions were performed up to 1% elongation.[16]

3. Results and Discussion

3.1. Young's Modulus Evaluation. Mechanical properties of spun fibers were determined by tensile tests. Stress−strain curves for some samples are shown in Figures 2−4 in which σ_{eng} and ϵ_{eng} indicate the engineering stress and strain, respectively. The low-strain region is exhibited in Figures 2 and 3. The latter shows the known effect of SDR on stiffness, while the former shows the effect of DMDBS content. A full stress−strain curve for one sample is shown in Figure 4. It indicates that these fibers can be subsequently drawn to a high cold draw ratio (CDR), which can lead to enhanced tensile modulus and other useful mechanical properties. A procedure utilizing nucleating agents in PP that permit high CDR in high-speed spinning has been reported recently in the patent literature.[14,15] The Young's moduli of the fabricated fibers are reported in Table 1. It indicates that the modulus peaks at a DMDBS level of 0.4%. Furthermore, PP/DMDBS fibers fabricated in the second temperature protocol (TP2) exhibited higher moduli. This is due to the fact that in this processing scheme the DMDBS crystals have not melted, so that during spinning these nanofibrous crystals orient during shear and elongation flow in and at the exit of the nozzle, respectively. Thus, the oriented fibrils serve as efficient nucleation sites for PP crystals, in oriented shish-kebab morphology, upon further cooling. Apparently, in the TP1 scheme, there is not sufficient time for DMDBS nanofibrils to form in the PP melt for proper orientation during the short residence time in the elongational flow beyond the nozzle. The reason for the maximal stiffness achieved at about 0.4% DMDBS is not clear. In shear-oriented samples the modulus increased continuously in the investigated additive content (up to 0.75%),[9] or the orientation was shown to continuously increase up to about 5% additive.[11] It may be that only at relatively low DMDBS content, at the TP2 conditions in which the nanofibrils do not melt, the fibrillar network can break into individual long thin nanofibrils which successfully orient in the flow.

Table 1. Young's Modulus of Fabricated Fibers (All Values in MPa)

	0% DMDBS	0.4% DMDBS	1% DMDBS
TP1 low SDR	580 ± 190	770 ± 180	200 ± 130
TP1 high SDR	1200 ± 310	1200 ± 190	970 ± 150
TP2 low SDR	500 ± 230	790 ± 350	770 ± 250
TP2 high SDR	1300 ± 470	1700 ± 260	1400 ± 490

3.2. WAXS Evaluations. The orientation of PP crystals is evaluated by X-ray diffraction. WAXS patterns taken from the various samples can be seen in Figure 5. In accord with the results of the mechanical evaluation, the 0.4% DMDBS system presents the highest orientation. Again TP2 systems present a preferable outcome. As systems with fiber orientation tend to exhibit shish-kebab morphology, the expectation from these WAXS patterns was to have only equatorial diffraction. However, as noted in Figure 5, this is clearly not the case. The existence of diffraction arcs from the 110 planes in the equatorial and off-meridian directions indicates the presence of two types of oriented α-PP crystals, with either *c*-axis or *a**-axis preferential orientation along the fiber (spinning) direction. The crystal lamellae are thus preferentially oriented with their lamellar normal either parallel or perpendicular to the fiber direction, as has been seen in undrawn PP filaments[17] and in the skin region of injection-molded PP under high-shear conditions.[18−20] These two types of orientation come to pass due to epitaxial growth[21,22] of "daughter" *a**-axis oriented PP lamellae on previously formed "mother" *c*-axis oriented lamellae.[19,20] Thus, the structure in the skin region of injection-molded PP under high stress has been interpreted as a "modified" shish-kebab morphology, whereby stress-oriented chains form the shish which nucleates the *c*-axis lamellae which further nucleate the *a**-axis lamellae. We can therefore envision that the semicrystalline morphology in the oriented fibers containing 0.4% DMDBS spun using the TP2 temperature protocol to be similar to the "modified" shish-kebab structure described above. At these conditions the nucleator fibrils are present intact during the orienting flow of the polymer melt and may partially replace the oriented "shish" structure as

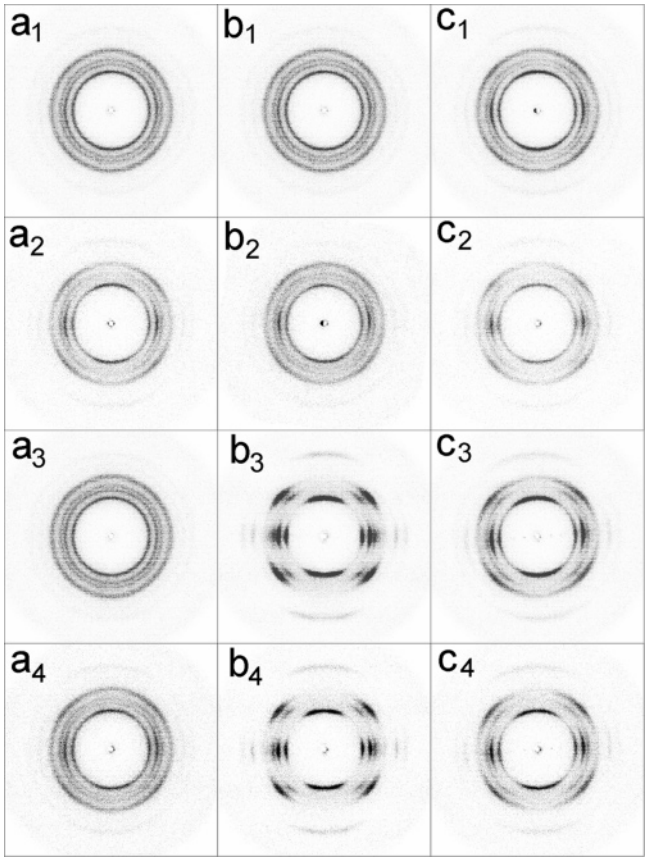

Figure 5. WAXS patterns obtained from different PP fibers. Letters denote DMDBS percentage: a, 0%; b, 0.4%; c, 1%. Numbers indicate preparation method: 1, first temperature protocol (TP1) low SDR; 2, TP1 high SDR; 3, second temperature protocol (TP2) low SDR; 4, TP2 high SDR.

Table 2. Fraction of Crystals with Preferential Orientation of the *c*-Axis along the Fiber Direction (F_f)

	0%	0.4%	1%
TP1 low SDR	0.05	0.03	0.04
TP1 high SDR	0.21	0.09	0.18
TP2 low SDR	0.05	0.37	0.16
TP2 high SDR	0.15	0.39	0.27

Table 3. *c*-Axis Orientation Factor (fc)

	0%	0.4%	1%
TP1 low SDR	0.43	0.38	0.70
TP1 high SDR	0.82	0.71	0.82
TP2 low SDR	0.52	0.95	0.85
TP2 high SDR	0.72	0.95	0.88

the nucleation sites for subsequent *c*-axis oriented lamellar crystallization.

In further analysis we focus on the fraction of crystals having preferred *c*-axis orientation along the fiber direction and the orientation degree of this fraction, as these are the dominant ones in quantity and in contribution to the stiffness. The fraction of *c*-axis oriented crystals (F_f) is obtained from the azimuthal plot of the 110 reflection by the ratio of the equatorial peak area to the total area (including *c*-axis and *a**-axis oriented crystals as well as nonoriented material, after subtraction of the low background noise).[19,20] The peak areas were integrated using the Lorentz correction as $\int I(\phi)\sin\phi \mathrm{d}\phi$, where ϕ is the azimuthal angle. The results of this evaluation are shown in Table 2, indicating the known effect of draw ratio on the amount of oriented crystals. Melt spinning of the fibers at higher take-up speeds in both temperature protocols resulted in higher fractions of *c*-axis oriented crystals. The highest fraction of *c*-axis oriented material is achieved in the filament with 0.4% DMDBS produced via the second temperature protocol (TP2).

The *c*-axis orientation factor (fc), relative to the fiber direction (*z*-axis), is calculated by[23]

$$fc = \frac{3\langle\cos^2\phi_{c,z}\rangle - 1}{2} \tag{1}$$

For PP the value of $\langle\cos^2\phi_{c,z}\rangle$ can be obtained from the values of $\langle\cos^2\phi_{hkl,z}\rangle$ measured from the equatorial arcs of the 110 and 040 planes, defined as[23]

$$\langle\cos^2\phi_{hkl,z}\rangle = \frac{\int_0^{\pi/2} I(\phi)\sin\phi\cos^2\phi\,\mathrm{d}\phi}{\int_0^{\pi/2} I(\phi)\sin\phi\,\mathrm{d}\phi} \tag{2}$$

by[23]

$$\langle\cos^2\phi_{c,z}\rangle = 1 - 1.099\langle\cos^2\phi_{110,z}\rangle - 0.901\langle\cos^2\phi_{040,z}\rangle \tag{3}$$

The calculated orientation factors are presented in Table 3. In the calculation (eq 3) we neglect the effect of the daughter (*a**) lamellae on the azimuthal breadth of the observed (040) reflection. This is a small effect lowering the calculated orientation factor, due to the low content of these less oriented crystals. These calculations show quantitatively the trends shown in Figure 5. As mentioned above, in the first processing scheme (TP1) the DMDBS nanofibrils are molten in the die, and hence no significant effect of the additive on orientation is observed. In the second temperature protocol (TP2), where the preexisting fibrillar structure can be oriented by the melt spinning process, there is clear evidence for maximal orientation at 0.4% DMDBS content, even at low draw ratio.

3.3. SAXS Evaluations. Fiber morphology was examined by small-angle X-ray scattering. SAXS patterns from the various samples can be seen in Figure 6. Meridional scattering reflections can be observed as rather broad lobes. As is known, these reflections are due to lamellar stacking. Sharper reflections are observed in samples exhibiting higher degrees of *c*-axis orientation, in accord with the WAXS patterns. The patterns from some samples also display second-order reflections, indicating a narrow size distribution of the long period of the lamellar stacks. These samples, marked as b_3 and c_3, in Figure 6, refer to fibers containing DMDBS at low draw ratio and spun from the lower temperature melt (TP2). Closer scrutiny of the patterns indicates that in these samples additional SAXS reflections occur also on the equator. The double-orientation morphology indicated by the presence of meridional and equatorial reflections in scattering from these samples has been related in previous studies to be due to epitaxial growth of daughter lamellae, as mentioned earlier.[21,22]

Calculations of the long period and the degree of crystallinity were performed on vertical cross section of the reflection lobes, whereas the lateral dimension of coherence in the lamellae was carried out on their horizontal cross section. The long period, *L*, and the degree of crystallinity, *Xc*, reported in Table 4, were calculated by Bragg's law, combined with the method of Tsvankin (see Supporting Information), which accounts also for the finite width of the crystalline/amorphous interface.[24] Table 4 suggests that the long period is unaffected by the fiber fabrication procedure or the presence of DMDBS. Neither does the degree of crystallinity.

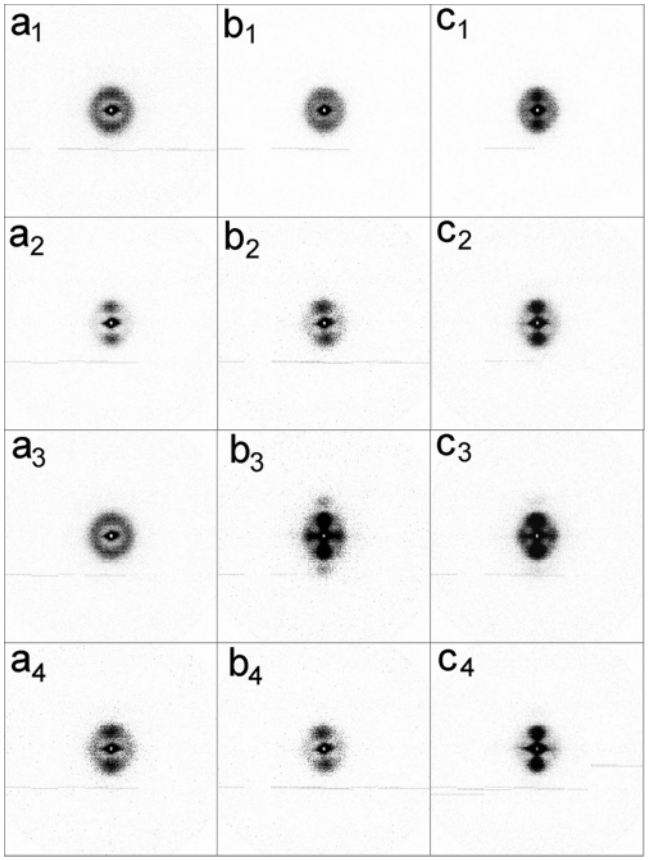

Figure 6. SAXS patterns obtained from different PP fibers. Letters denote DMDBS percentage: a, 0%; b, 0.4%; c, 1%. Numbers indicate preparation method: 1, TP1 low SDR; 2, TP1 high SDR; 3, TP2 low SDR; 4, TP2 high SDR.

Table 4. Long Period and Degree of Crystallinity

	0% DMDBS		0.4% DMDBS		1% DMDBS	
	L (nm)	*Xc*	*L* (nm)	*Xc*	*L* (nm)	*Xc*
TP1 low SDR	12	0.62	14	0.58	14	0.60
TP1 high SDR	12	0.65	12	0.63	13	0.63
TP2 low SDR	12	0.61	15	0.59	14	0.60
TP2 high SDR	12	0.64	14	0.60	13	0.62

Table 5. Lateral Dimensions (in nm) of Coherently Scattering Region of the Lamellae

	0% DMDBS	0.4% DMDBS	1% DMDBS
TP1 low SDR	8	8	13
TP1 high SDR	14	14	17
TP2 low SDR	6	41	22
TP2 high SDR	12	42	21

For comparison purposes, the lateral dimensions of coherently scattering region of the lamellae, given in Table 5, were evaluated by the reciprocal of the horizontal breadth of the meridional SAXS reflections, determined by the full width at half-maximum of the peak intensity (fwhm). Again, fibers fabricated with 0.4% DMDBS at TP2 protocol exhibit the best values in this respect.

4. Conclusions

This work examined the influence of DMDBS, at two different concentrations (0.4 and 1%), on oriented PP fibers. The fibers were fabricated at two spin draw ratios (about 20 and 180) and by two temperature protocols, providing differing conditions for fibrillar structure formation. In the first protocol, where the melt was heated up to 220 °C, conditions were provided for the complete melting and dissolving of DMDBS. The second protocol with a melt temperature of no more than 180 °C assumingly kept the preexisting fibrillar structure intact. Tensile properties were correlated with morphological characteristics of the PP crystals evaluated by small- and wide-angle X-ray scattering. The results show a higher tensile modulus at 0.4% DMDBS, likely due to better orientation of the PP crystals along the fiber direction. It is hypothesized that for enhanced orientation it is necessary to have DMDBS nanofibrils during the shear flow in the die and elongational flow of the PP melt at and beyond the nozzle exit. The oriented nanofibrils can then serve as nucleation sites for oriented PP crystallization, most likely in a shish-kebab morphology. Moreover, a double-orientation structure is observed, suggesting the modified shish-kebab morphology whereby daughter lamellae oriented with their normals along the radial direction are epitaxially grown on the kebab lamellae, the normals of which are oriented along the fiber direction. These results highlight the importance of the proper fabrication temperature protocol which can provide for the preexisting DMDBS fibrillar structure to remain intact during the melt spinning process. The reason for the better performance of the fibers with DMDBS content of about 0.4% is unclear. It can be hypothesized that at low DMDBS concentrations the fibrillar structure is composed mainly of long easily stretched and oriented nanofibrills providing a good template for polymer chain alignment, whereas at higher DMDBS content more branched and less oriented structures may form in the melt.

Supporting Information Available: Evaluation of the degree of crystallinity by small-angle X-ray scattering using Tsvankin's method.[24] This material is available free of charge via the Internet at http://pubs.acs.org.

References and Notes

(1) Terech, P.; Weiss, R. G. *Chem. Rev.* **1997**, *97*, 3133.
(2) Fillon, B.; Lotz, B.; Thierry, A.; Wittmann, J. C. *J. Polym. Sci., Part B: Polym. Phys.* **1993**, *31*, 1395.
(3) Shepard, T. A.; Delsorbo, C. R.; Louth, R. M.; Walborn, J. L.; Norman, D. A.; Harvey, N. G.; Spontak, R. J. *J. Polym. Sci., Part B: Polym. Phys.* **1997**, *35*, 2617.
(4) Wilder, E. A.; Hall, C. K.; Khan, S. A.; Spontak, R. J. *Recent Res. Dev. Mater. Sci.* **2002**, *3*, 93.
(5) Takenaka, M.; Kobayashi, T.; Hashimoto, T.; Takahashi, M. *Phys. Rev. E* **2002**, *65*, 0414011.
(6) Kobayashi, T.; Hashimoto, T. *Bull. Chem. Soc. Jpn.* **2005**, *78*, 218.
(7) Thierry, A.; Straupe, C.; Lotz, B.; Wittmann, J. C. *Polym. Commun.* **1990**, *31*, 299.
(8) Kristiansen, M.; Werner, M.; Tervoort, T.; Smith, P.; Blomenhofer, M.; Schmidt, H. W. *Macromolecules* **2003**, *36*, 5150.
(9) Shepard, T. A.; Delsorbo, C. R.; Louth, R. M.; Walborn, J. L.; Norman, D. A.; Harvey, N. G.; Spontak, R. J. *J. Polym. Sci., Part B: Polym. Phys.* **1997**, *35*, 2617.
(10) Nogales, A.; Olley, R. H.; Mitchell, G. R. *Macromol. Rapid Commun.* **2003**, *24*, 496.
(11) Nogales, A.; Mitchell, G. R.; Vaughan, A. S. *Macromolecules* **2003**, *36*, 4898.
(12) Nogales, A.; Mitchell, G. R. *Polymer* **2005**, *46*, 5615.
(13) Wangsoub, S.; Olley, R. H.; Mitchell, G. R. *Macromol. Chem. Phys.* **2005**, *206*, 1826.
(14) Morin, B. G.; Royer, J.; Burkhart, B. M. United States Patent 6,878, 443, April 12, 2005.
(15) Cowan, M. E.; Morin, B. G. United States Patent 7,041,368, May 9, 2006.
(16) Karger-Kocsis, J. *Polypropylene Structure, Blends and Composites*, 1st ed.; Chapman & Hall: London, 1995; Vol. 2, Chapter 5.
(17) Katayama, K.; Amano, T.; Nakamura, K. *Kolloid Z. Z. Polym.* **1968**, *226*, 125.
(18) Clark, E. S.; Spruiell, J. E. *Polym. Eng. Sci.* **1976**, *16*, 176.
(19) Fujiyama, M.; Wakino, T.; Kawasaki, Y. *J. Appl. Polym. Sci.* **1988**, *35*, 29.

(20) Karger-Kocsis, J. *Polypropylene Structure, Blends and Composites*, 1st ed.; Chapman & Hall: London, 1995; Vol. 1.
(21) Lotz, B.; Wittmann, J. C. *J. Polym. Sci., Polym. Phys. Ed.* **1986**, *24*, 1541.
(22) Lotz, B.; Wittmann, J. C.; Lovinger, A. J. *Polymer* **1996**, *37*, 4979.
(23) Alexander, L. E. *X-Ray Diffraction Methods in Polymer Science*; Wiley-Interscience: New York, 1969; Chapter 4.
(24) Tsvankin, D. Ya. *Polym. Sci. USSR* **1964**, *6*, 2304.

MA071387U